Analysis of Displacement Fields near Dislocation Cores in Ordered Polymers

Lawrence F. Drummy,[†] Ingrid Voigt-Martin,[‡] and David C. Martin*[,†]

Materials Science and Engineering and the Macromolecular Science and Engineering Center, The University of Michigan, Ann Arbor, Michigan 48109-1055, and the Institute for Physical Chemistry, The University of Mainz, Mainz, Germany

Received January 2, 2001; Revised Manuscript Received June 4, 2001

ABSTRACT: We have significantly improved a method to characterize the displacement fields near edge dislocations in ordered polymers. Our extended analysis now makes it possible to predict and explain the variation in tilt of different lattice planes in the vicinity of dislocations in isotropic solids, anisotropic crystals, and liquid crystals in terms of their elasticity constants. Direct images of the dislocation cores were obtained in three different polymer systems using bright field transmission electron microscopy (TEM) and high-resolution electron microscopy (HREM). A $b[010] = 63$ nm edge dislocation was imaged in the ABC triblock copolymer polystyrene-*block*-poly(ethylene-*co*-butylene)-*block*-poly(methyl methacrylate) (SEBM). The isotropic displacement fields according to theories by Taylor and Burgers were compared to the SEBM data. Fitting the theoretical displacement fields to the displacements measured from the image, an estimate of the elastic constant anisotropy was obtained. For this material the ratio of the bulk modulus to the shear modulus, K/G, was equal to 0.8 ± 0.2. A similar analysis using anisotropic dislocation theory was applied to a three chain-end, $b[200] = 2.4$ nm edge dislocation in the crystalline polymer [1,6-di(*N*-carbazolyl)-2,4-hexadiyne] (DCHD). Information about the anisotropy of DCHDs stiffness matrix, C_{ij}, was obtained. An anisotropy parameter W_2, defined as $(C_{11} + C_{33})/(2C_{55})$, was found to be 3.0 ± 0.1. Finally, a $b = 2.6$ nm dislocation in a smectic polymalonate was analyzed using liquid crystalline dislocation theory. An estimate of λ, the material's characteristic deformation length, was determined to be 1.1 ± 0.1 nm.

Introduction

Defects in inorganic crystalline materials have been studied extensively due to their profound effect on macroscopic material properties. Similar studies in organic materials have been much more limited because of the difficulties in obtaining information about the details of their structure at the molecular level. Characterization of polymer microstructure using high-resolution electron microscopy (HREM) has only recently been developed as a tool for studying defects. Details on the use of low-dose HREM methods for the study of defects in polymers have been published elsewhere.[1−6]

The role of dislocations in the deformation of crystalline materials is well established. It has been acknowledged that the extent of localization of the dislocation core has a strong effect on plastic deformation.[7] It is the bonding anisotropy of the crystal that controls this localization. Studies done on talc, graphite, and nonbasal hcp dislocations have investigated the effects of strong anisotropy on dislocation core structure.[8,9] Crystalline polymers are also highly anisotropic, and it is expected that their dislocation structures will also exhibit variations in the degree of localization and other distortions in the lattice.

The applications of crystalline and semicrystalline polymers have grown to include uses in structural materials, high-strength fibers, and thin-film transistors. Characterizing the types of defects that form in polymers aids in the understanding of which will likely have the greatest influence on properties.[10−12] A better fundamental understanding of these defects is necessary to control material performance and motivate the development of more sophisticated molecular designs and processing schemes.

Yielding in semicrystalline polymers was first explained as a defect-controlled process by Peterson[13] and later by Young.[14,15] Both models took into account the thermal activation and slip of screw dislocations in the crystal platelets with Burgers vectors parallel to the polymer chain. A large amount of data on the plastic deformation of polyethylene, polypropylene, and nylon has been used to support the screw dislocation model since its proposal. Recent research suggests that Young's model is most applicable below a transition temperature associated with the β-relaxation temperature. In this new study, the energy of the dislocation core was assumed to be a function of temperature. With the use of this model, the yielding behavior of polyethylene was predicted over a wide range of temperatures and crystallite sizes.[16]

With careful examination of displacements near dislocation cores, it is possible to reveal details about the preferred deformation mechanisms of the material. In particular, information about the elastic constant anisotropy of the material can be extracted from images of these defects by measuring the molecular orientation near the core. Past studies have used direct images of disclinations and dislocations in liquid crystalline polymers to determine material elastic constants. Hudson and Thomas have investigated Frank elastic constant anisotropy with the use of TEM images of disclinations in nematic liquid crystalline polymers.[17,18] By measuring the molecular orientations near the disclination, they were able to determine values for k_{33}/k_{11}, the ratio of the bend constant to the splay constant, by comparison

[†] The University of Michigan.
[‡] The University of Mainz.
* Corresponding author.

10.1021/ma010003b CCC: $20.00
Published on Web 09/15/2001

with predicted deformation fields from liquid crystalline elasticity theory. It was found that for low bending constant polymers most of the bending deformation was localized near the defect. These results have been corroborated by numerical modeling of liquid crystal microstructure under strain. Hobdell and Windle[19] emphasized that the lower the elastic constant for a particular type of deformation, the more localized that deformation would be near a defect.

Ries et al.[20] used a similar approach to determine λ, the characteristic deformation length, from HREM lattice images of edge dislocations in the hexagonal columnar phase of phthalocyaninatopoly(siloxane) (PCPS). Here it was found that the bending modulus, K_3, was much less than the elastic modulus ($K_3/E = 0.04$ nm^2).

Molecular simulations have been successfully employed in the study of dislocation cores in organic molecular crystals such as anthracene[21] and naphthalene.[22] Our lab has recently modeled edge dislocations with Burgers vectors parallel to the polymer chain in DCHD.[23] Estimates of the system energies with increasing defect densities were obtained.

We have studied direct images of dislocation cores in crystalline polymers and compared them with the deformation fields predicted by anisotropic dislocation theory. Wilson and Martin[24] previously focused on chain-end edge dislocations in DCHD. The analysis was based on the correlation between θ, the tilt of the polymer chains near a dislocation, and ϵ_{xy}, the local shear strain. The shear strain field around an anisotropic dislocation can be solved with the 36 constant stiffness matrix of the crystal, C_{ij}, and the Burgers vector of the dislocation b. In the previous study the tilt of the polymer chains was measured azimuthally at a constant radius from the dislocation core ($r = 5b$) and compared to the shear strain predicted from theory. A best fit of the model dislocation to the data was obtained for a highly anisotropic stiffness matrix. It was concluded that the mechanical rigidity of DCHD's polymer backbone outweighed all other stiffness parameters and had the greatest influence on the dislocation core structure.

With the extension of the analysis to dislocations in isotropic materials, it became clear that the chain-end dislocation in DCHD was a unique case, and the direct relationship between tilt and shear strain did not hold in general. As we will demonstrate here in detail, the shear strain is a good approximation to the tilt only in certain situations, and in the general case the displacement fields must be used to predict lattice plane tilt near a dislocation.

We have now developed a method to determine the displacement fields near edge dislocation cores in various polymer systems by measuring lattice plane tilt. The analysis has proven useful to extract material parameters such as elastic constants from HREM images of dislocations. It has also given insight into the role of the microstructural arrangement and bonding of the polymer chains in the dislocation core structure. The materials studied include an ABC triblock copolymer showing the so-called knitted morphology, a single crystalline polydiacetylene droplet, and a smectic liquid crystal.

Experimental Section

Three different samples were investigated:

(1) The block copolymer polystyrene-*block*-poly(ethylene-*co*-butylene)-*block*-poly(methyl methacrylate) (SEBM). The volume fractions of polystyrene, poly(ethylene-*co*-butylene), and poly(methyl methacrylate) used to form this morphology were 0.36, 0.31, and 0.33, respectively. Details on the synthesis can be found elsewhere.[25] Thin sections of the block copolymer were obtained using an ultramicrotome equipped with a diamond knife and collected for TEM observation. The samples were stained with RuO_4. Bright field TEM was done using a Phillips transmission electron microscope operating at 80 kV and a JEOL 200 CX operating at 100 kV.

(2) The carbazolyl-substituted diacetylene polymer [1,6-di-(*N*-carbazolyl)-2,4-hexadiyene] (DCHD). Single-crystal textured droplets of DCHD were prepared for HREM examination. A 0.01 wt % solution of DCHD monomer in chloroform was deposited onto carbon-coated mica substrates. The carbon film was then floated onto deionized water for collection onto copper grids.[26] Samples were polymerized thermally at 150 °C for approximately 24 h.[27]

HREM images of DCHD droplets were taken using a JEOL 4000 EX transmission electron microscope operated at 400 kV. Images were obtained using low-dose methods to minimize the effects of electron beam irradiation.[2,3] Typical images were taken at a magnification of 100K× at a screen current of 20 pA/cm^2 with an exposure time of 1 s. These conditions result in a total electron dose at the sample of 0.2 C/cm^2.

(3) The main chain/side group liquid crystalline polymer was a polymalonate with azobenzene as the mesogenic groups in the main chain and cyanoazobenzene as the mesogenic side groups.[28] The films were prepared by solution casting, using a 0.1% solution in chloroform. Subsequent annealing close to the smectic−isotropic transition temperature caused orientation of the mesogenic groups.

Theory

When a body is acted upon by a stress, the displacement at a certain point in three dimensions can be expressed in terms of the displacement fields u, v, and w corresponding to displacements in the x, y, and z directions, respectively. For an edge dislocation with a dislocation line along the z direction, $w = 0$. The displacement fields u and v have been derived for a straight edge dislocation in an infinite crystal using linear elasticity, and the equations of static equilibrium specifying that the internal forces created by the dislocation give the deforming body no net momentum. Also used in the derivation is the compatibility equation, which imposes that certain strains cannot be assumed to be independent of each other, yet must be expressed in terms two displacement fields. These displacement fields were derived and applied to edge dislocations by Taylor.[29] They have been referred to by several authors[30−32] in their work on edge dislocations, and they can be used to describe a "Taylor dislocation".

$$u = \frac{b}{2\pi}\left[\phi + \frac{\lambda+\mu}{2(\lambda+2\mu)}\sin[2\phi]\right] = \frac{b}{2\pi}\left[\arctan\left[\frac{y}{x}\right] + \frac{\lambda+\mu}{\lambda+2\mu}\frac{xy}{x^2+y^2}\right] \quad (1a)$$

$$v = -\frac{b}{2\pi}\left[\frac{\mu \ln r}{\lambda+2\mu} + \frac{\lambda+\mu}{2(\lambda+2\mu)}\cos[2\phi]\right] = -\frac{b}{2\pi}\left[\frac{\mu}{2(\lambda+2\mu)}\ln(x^2+y^2) + \frac{\lambda+\mu}{2(\lambda+2\mu)}\frac{x^2-y^2}{x^2+y^2}\right] \quad (1b)$$

Figure 1a depicts a model edge dislocation formed with the theoretical displacement fields above. They differ from the displacement fields in the analysis later developed by Burgers.[33] Authors have used this second,

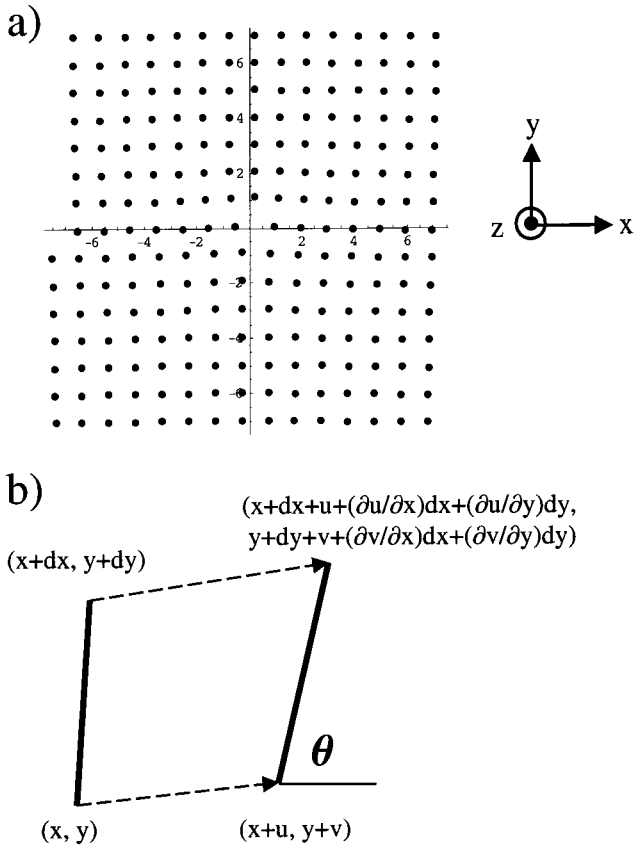

Figure 1. (a) Lattice map of a $b[100] = 1$ nm edge dislocation formed using the isotropic displacement fields u and v, setting $\lambda/\mu = 1$. Axes are in nanometers. (b) Schematic of the method used to predict tilt (θ) of any lattice plane given by dx and dy around a dislocation whose displacement fields are given by u and v.

distinct set of displacement fields to describe a "Burgers dislocation".[34−36] The difference between the two lies in the second term in the expression for v, which is modified from Taylor's original solution so that a finite crystal containing an edge dislocation exists at equilibrium with no force exerted on the surfaces. We are now in a position to investigate the differences between the two sets of displacement fields and determine which one can most appropriately describe an edge dislocation in an isotropic polymeric material. The displacement fields according to Burgers are

$$u[x,y] = \frac{b}{2\pi}\left[\arctan\left[\frac{y}{x}\right] + \frac{\lambda+\mu}{\lambda+2\mu}\frac{xy}{x^2+y^2}\right] \quad (2a)$$

$$v[x,y] = -\frac{b}{2\pi}\left[\frac{\mu}{2(\lambda+2\mu)}\ln(x^2+y^2) + \frac{\lambda+\mu}{2(\lambda+2\mu)}\frac{x^2}{x^2+y^2}\right] \quad (2b)$$

We will demonstrate that the difference between the Taylor and Burgers dislocation is small outside of the dislocation core; however, the Taylor dislocation proves to be a better fit to the data measured from an edge dislocation in isotropic block copolymer SEBM.

To calculate the displacement fields for an isolated edge dislocation in an isotropic material, the necessary parameters are the magnitude of the Burgers vector, $|\mathbf{b}|$, and the Lamé constants, λ and μ. From u and v the tilt of any line element, or unit cell plane, at any point

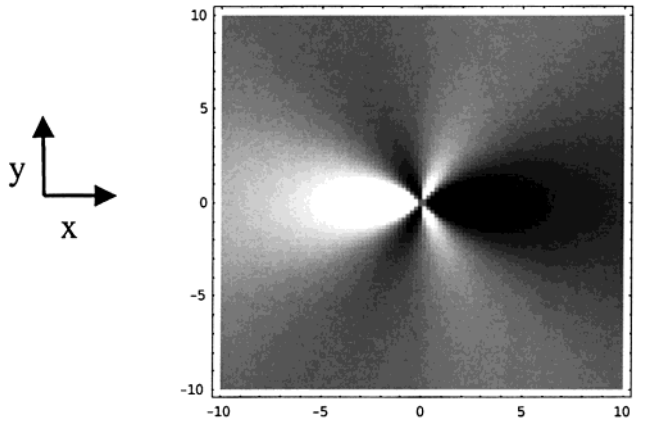

Figure 2. Density plot of the shear strain, ϵ_{xy}, near a $b[100] = 1$ nm edge dislocation. Axes are in nanometers.

near an isolated dislocation can be calculated. A schematic of the method to determine lattice plane tilt is shown in Figure 1b. θ is then defined as

$$\theta = \arctan\left[\frac{dy + \frac{\partial v}{\partial x}dx + \frac{\partial v}{\partial y}dy}{dx + \frac{\partial u}{\partial x}dx + \frac{\partial u}{\partial y}dy}\right] \quad (3)$$

Our previous analysis directly related the tilt of the polymer chain to the local shear strain.[24] As we will demonstrate, in certain cases (such as highly rigid chains) this proves to be a good approximation. For an edge dislocation line along z with Burgers vector b in the x direction, the shear strain is defined as[37]

$$\epsilon_{xy} = \frac{b}{4\pi(1-\nu)}\frac{x(x^2-y^2)}{(x^2+y^2)^2} \quad (4)$$

where λ and μ are the Lamé constants and ν, Poisson's ratio, is equal to $\lambda/2(\lambda+\mu)$. For a dislocation of the orientation shown in Figure 1a, the functional form of the shear strain field can be seen as a density plot in two-dimensional space in Figure 2. The tilt of the (100) planes, the planes normal to the x direction, do not generally conform to this behavior, however, as was previously hypothesized. In particular, the small lobes present above and below the slip plane are not seen in the tilt measured from experimental images of dislocations. The shear strain and rigid rotations caused by an edge dislocation can be expressed in terms of derivatives of the displacement fields.

$$\epsilon_{xy} = \frac{1}{2}\left(\frac{\partial u}{\partial y} + \frac{\partial v}{\partial x}\right) \quad (5)$$

$$\omega_{xy} = \frac{1}{2}\left(\frac{\partial u}{\partial y} - \frac{\partial v}{\partial x}\right) \quad (6)$$

To predict the tilt of the (100) planes near a $b[100]$ edge dislocation, both the shear strains and rigid rotations must be accounted for. The shear strain is a good approximation to the tilt of the (100) planes only when dv/dx approaches zero. For anisotropic crystals that are stiff along the y direction, such as the crystalline polymer DCHD previously studied, this approximation will hold. DCHD is covalently bonded along the polymer chain and has relatively weak lateral interactions. In this case, displacements along y are limited, and there-

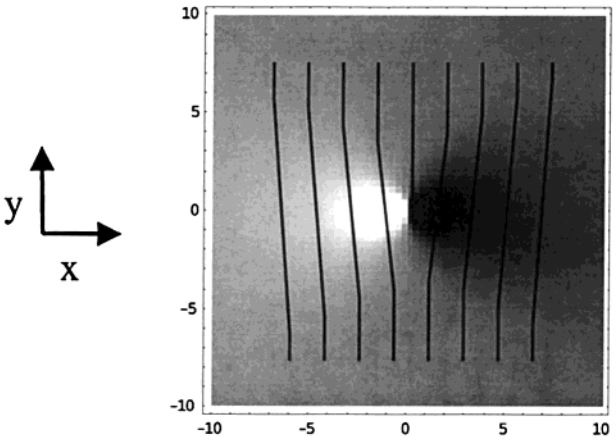

Figure 3. Density plot of the theoretical tilt field, $\theta[x,y]$, of the [100] planes near a $b[100] = 1$ nm edge dislocation calculated using the method described in Figure 1b. The dislocation orientation, with the Burgers vector in the x direction, is overlaid. Axes are in nanometers.

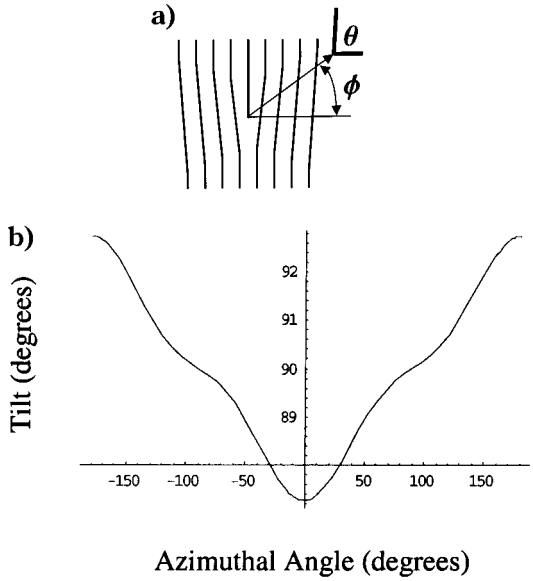

Figure 4. (a) Schematic of the method used to measure tilt (θ) of the crystallographic planes as a function of azimuthal angle from experimental images of edge dislocations. (b) [100] theoretical tilt vs azimuthal angle in polar space at a radius of 5b.

fore the magnitudes of the derivatives of v are negligible. However, extending the analysis to more isotropic materials shows that subtle variations in dv/dx near the core of edge dislocations cannot be ignored. In fact, we have found that the magnitude of dv/dx can be as great as 50% of the magnitude of du/dy near a $b[100]$ edge dislocation in an isotropic material.

The predicted tilt field, $\theta[x,y]$, of the (100) planes around a $b[100] = 1$ nm edge dislocation in an isotropic body is shown as a density plot in Figure 3. The magnitude of tilt in $x-y$ space near the dislocation core is plotted using the above method by setting d$x = 0$ and d$y = 1$. Tilt of the polymer lattice planes can be measured from experimental images of dislocations at varying azimuthal angle ϕ and constant radius r from the dislocation core. A schematic of this measurement technique is shown in Figure 4a. Theoretically predicted tilt can also be plotted for comparison with distortions measured from the images. Figure 4b shows the tilt distribution of the (100) planes for a $b[100] = 1$ nm edge

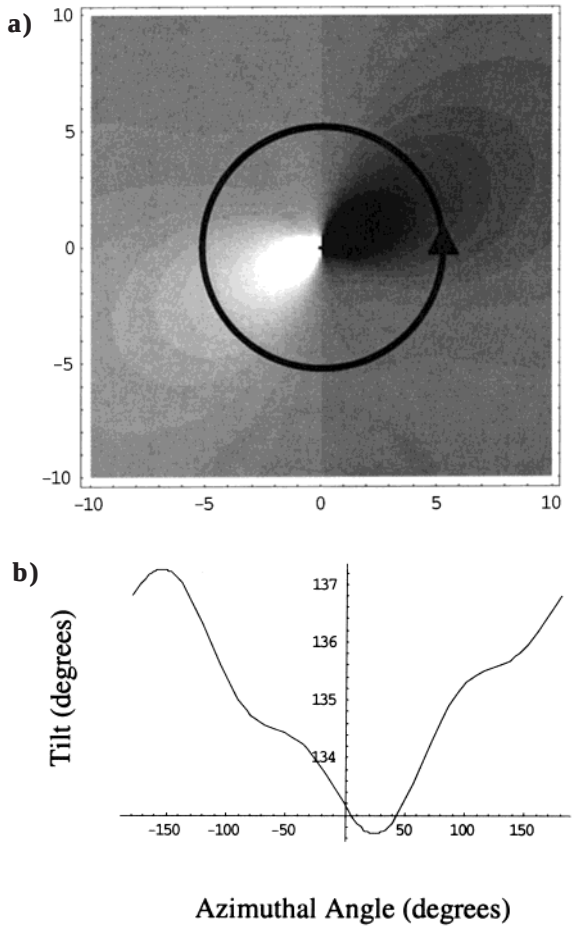

Figure 5. (a) Theoretical tilt of the [110] planes in x, y space near a $b[100] = 1$ nm edge dislocation shown as a density plot. Axes are in nanometers. Gray scale: white > 140°, black < 130°. (b) [110] theoretical tilt vs azimuthal angle in polar space at a raduis of 5b.

dislocation in polar space at a radius of five Burgers vectors from the core. Using this method, we can predict the tilt distribution of any set of planes around a dislocation in any crystallographic orientation. By setting d$x = -1$ and d$y = 1$, we can examine the predicted tilt of the (110) planes near a $b[100]$ edge dislocation. The density plot and corresponding tilt vs ϕ plot at $r = 5b$ are shown in Figure 5a,b. Note the asymmetry of the tilt distribution about $\phi = 0°$ and 180°.

For a dislocation of a given Burgers vector, the Lamé constants λ and μ are the only parameters that influence the displacement field solutions of an isotropic dislocation. λ and μ can be related to K, the bulk modulus, and G, the shear modulus, by the following equation, where d is the dimensionality of the deformation:[32]

$$\frac{K}{G} = \frac{\lambda}{\mu} + \frac{2}{d} \tag{7}$$

For the case of a straight edge dislocation, $d = 2$, giving $K/G = \lambda/\mu + 1$. Figures 6 and 7 illustrate the effect that the competing elastic constants, K and G, have on the way the displacements of an edge dislocation are accommodated in an isotropic material. An edge dislocation disrupts the translational symmetry of a material at the core by generating lattice plane tilt as well as local volumetric deformation. For a material with $K \gg G$, bulk deformation is more energetically costly than shear deformation. In this case, most of the shear

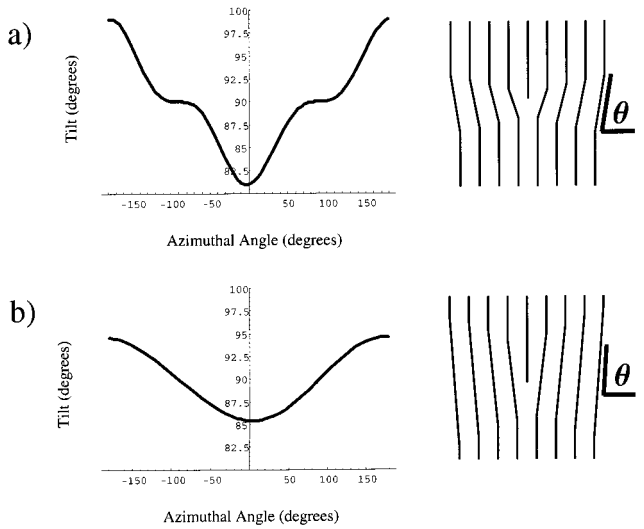

Figure 6. Predicted tilt of the (100) planes vs azimuthal angle at $r = 2b$ shown with a schematic of the deformation of those planes near a b[100] dislocation. (a) $K \gg G$ and (b) $G \gg K$.

deformation would be concentrated near the core of the dislocation, while bulk deformation would be spread out. The reverse is true for a material with $G \gg K$. These phenomena can be seen in Figure 6. For $K \gg G$, the tilt of the (100) planes calculated from isotropic theory is shown in Figure 6a vs azimuthal angle at $r = 2b$, along with a schematic of the deformation of those planes. Much of the tilt deformation is concentrated near the slip plane at $\phi = 0°$ and $\phi = 180°$. Figure 6b shows the deformation response when $G \gg K$. Here, tilt deformation is more energetically costly, and hence it is spread out in polar space. The material is able to deform in this manner only at the cost of producing large amounts of tension and compression localized near the dislocation core.

To study this local tension and compression further, we can use the displacement fields to calculate the change in length, ΔL, of any set of lattice planes near a dislocation. Figure 7 depicts the method used to calculate ΔL, along with density plots of $\Delta L(100) + \Delta L(010)$. For a material with $G \gg K$, bulk deformation is favored, and large amounts of tension and compression are localized near the defect. However, for $K \gg G$, bulk deformation is nearly absent. The change in length of any lattice plane, ΔL, is

$$\Delta L = \left[\left(dx + \left(\frac{\partial u}{\partial x}\right)dx + \left(\frac{\partial u}{\partial y}\right)dy\right)^2 + \left(dy + \left(\frac{\partial v}{\partial x}\right)dx + \left(\frac{\partial v}{\partial y}\right)dy\right)^2\right]^{1/2} - [dx^2 + dy^2]^{1/2} \quad (8)$$

Linear elastic dislocation theory predicts that the magnitude of tilt distortions scale as $1/r$ moving away from the core in any direction. Linear elasticity also predicts that distortions go to infinity at the core. Traditional dislocation theory uses a cutoff radius, r_0, inside of which linear elasticity breaks down. Inside r_0 the discrete nature of the lattice becomes dominant, and

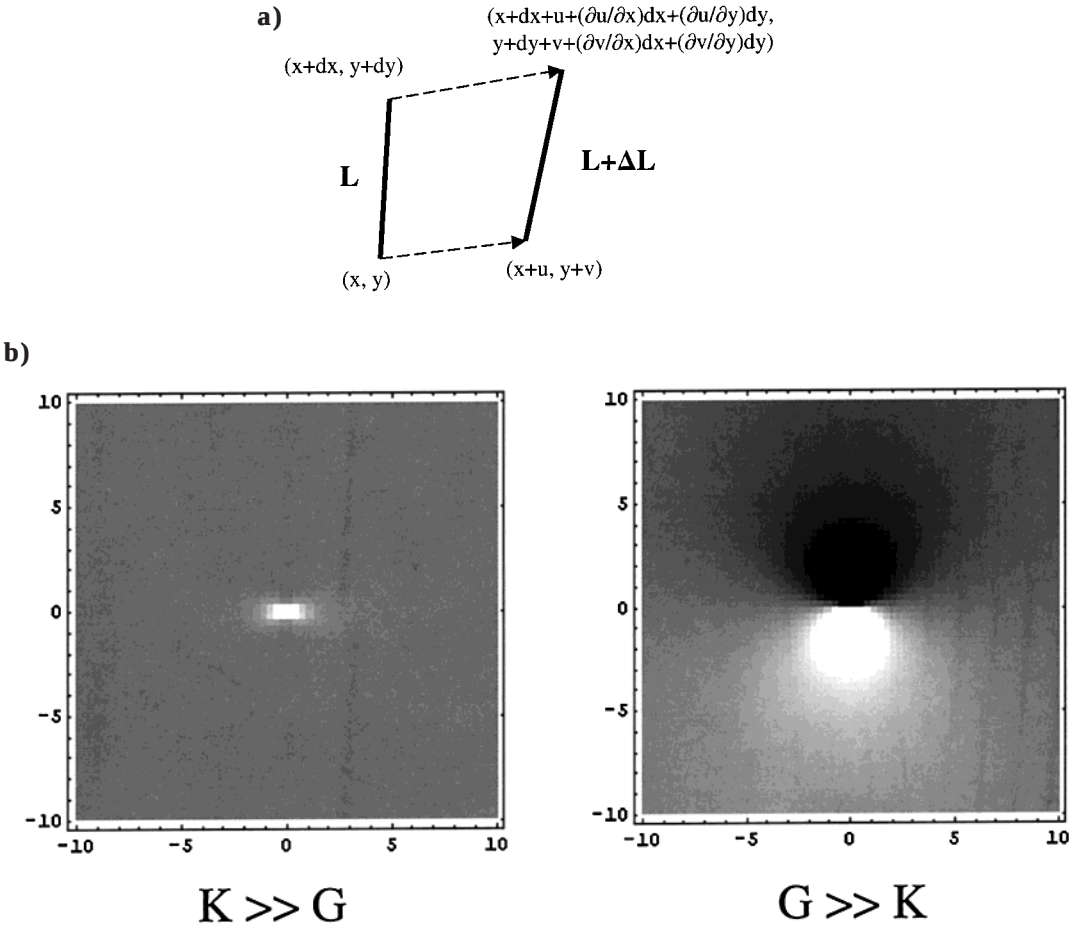

Figure 7. (a) Schematic of the method used to calculate the change in length ΔL of any set of planes near a dislocation with displacement fields u and v. (b) Density plots of $\Delta L(100) + \Delta L(010)$ near a b[100] = 1 nm edge dislocation. Axes are given in nm. Gray scale: white > +10%, black < −10%.

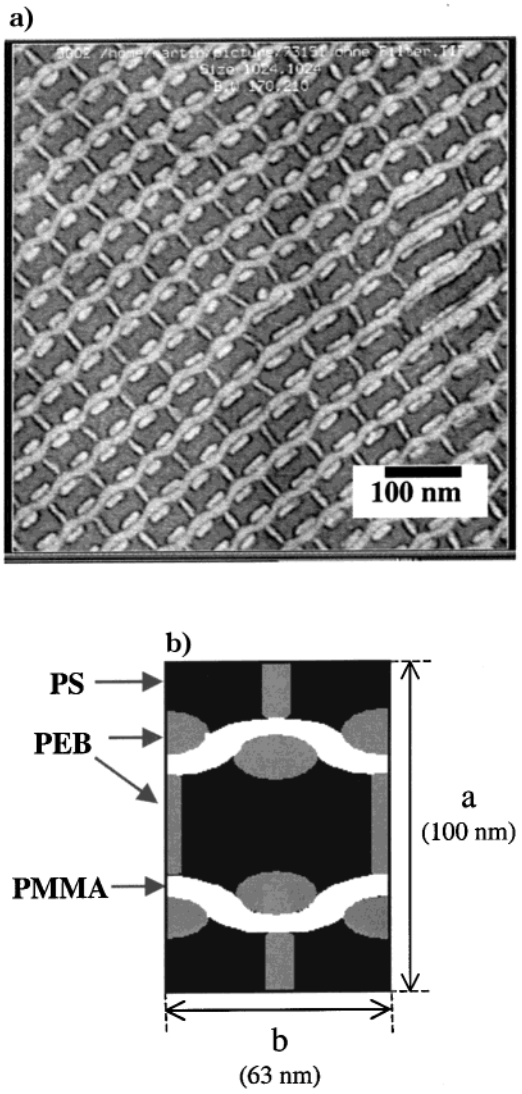

Figure 8. (a) The "knitted" morphology of the triblock copolymer that forms under certain polymerization conditions. (b) The unit cell depicting the microphase separation of the polystyrene, poly(ethylene-*co*-butylene), and poly(methyl methacrylate) blocks.

displacements are nonlinear. The goal of this paper is to investigate our ability to apply linear elastic dislocation theory to direct images of dislocations in various polymer systems.

Dislocations in ABC Triblock Copolymers

Polystyrene-*block*-poly(ethylene-*co*-butylene)-*block*-poly(methyl methacrylate) forms a unique "knitted" morphology.[38] Figure 8 shows a TEM image of the microstructure, along with the unit cell dimensions determined from small-angle X-ray scattering studies. The unit cell contents and lattice defects can be determined by electron microscopy. This unique morphology allows individual dislocations present to be studied in depth at reasonably high resolution. The electron micrographs show the distortions of the lattice around the dislocation core directly and when analyzed give information about the elastic constants of the material. Each unit cell contains two glide planes and two mirror planes in each direction, corresponding to symmetry of C_{2mm}. A $b[010] = 63$ nm edge dislocation is shown in this material in Figure 9a. We chose to study the (020) and (220) planes near the dislocation. Two-dimensional polar

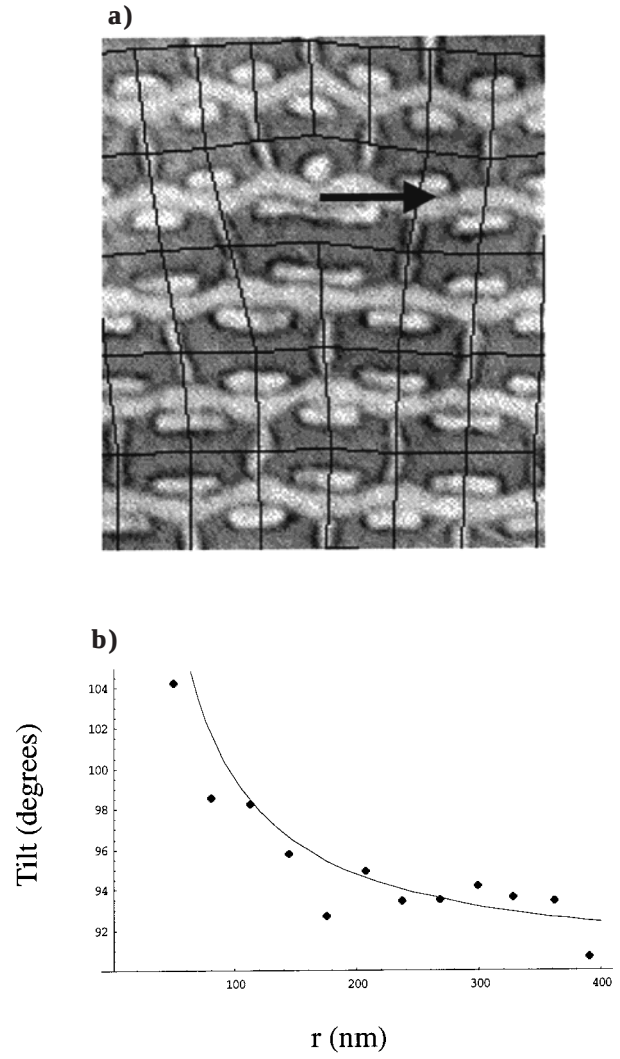

Figure 9. (a) The dislocation core, with the (200) and (020) planes drawn in. (b) Tilt of the (020) planes vs distance from the core, r, at $\phi = 180°$. The data points represent tilt of the (020) planes measured from the image.

coordinates (r,ϕ) were used in the analysis to plot tilt (θ) as a function of r holding ϕ constant or to plot tilt as a function of ϕ holding r constant.

Using the above method to predict the tilt of the (020) planes, we find that the tilt conforms well to the predicted $1/r$ dependence. (Figure 9b) By plotting (020) tilt azimuthally around the core at constant r, we can begin to see where most of the tilt distortions are contained in polar space near the dislocation. Figure 10 shows tilt of the (020) planes vs azimuthal angle, theoretical and experimental, at a distance of one Burgers vector.

The data reveals that the material behaves essentially isotropically in its response to a dislocation, and an estimate of λ/μ can be obtained. For a given value of λ/μ, an rms error can defined to determine the quality of fit of the theoretical tilt predictions to the corresponding data set. Adding up the calculated R factors for every data set from an image, we obtain a total rms error for a particular value of λ/μ. The rms error of a particular data set can be defined as

$$\text{rms error} = \frac{1}{N}\left(\sum_{i=1}^{N}(\theta_{\text{data}} - \theta_{\text{theory}})^2\right)^{1/2} \qquad (9)$$

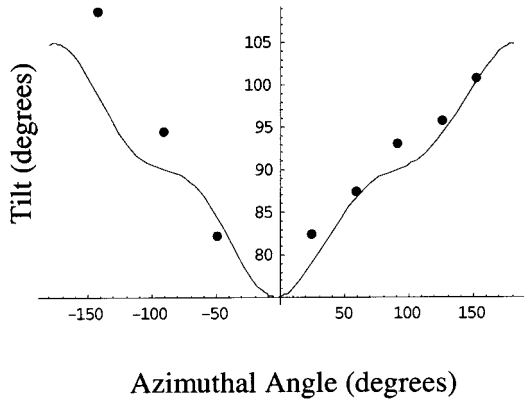

Figure 10. Tilt of the (020) planes vs azimuthal angle at $r = 1b$.

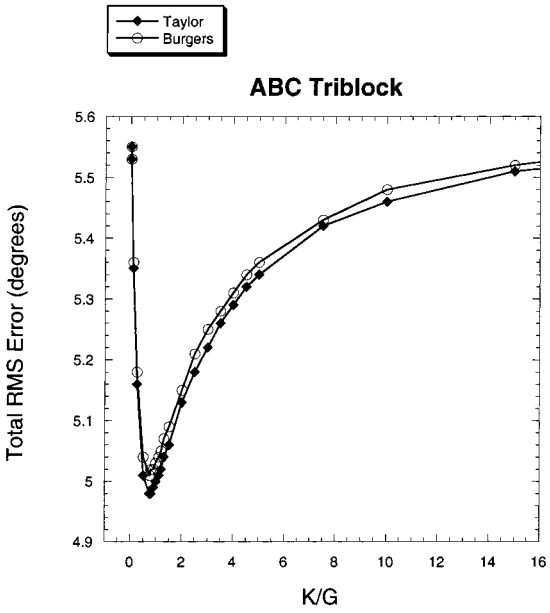

Figure 11. Total rms error of the fit with varying K/G calculated using the displacement fields according to Taylor and Burgers summed up over six data sets.

where θ_{data} is the tilt measured from the image, θ_{theory} is the corresponding predicted tilt, and N is the number of data points in the set. Using the above equation, we can extract a value for K/G by determining the minimum total rms error. Figure 11 shows the total rms error added up from six data sets such as those in Figures 9b and 10 at various values of K/G. The predicted tilt values are calculated from both sets of displacement fields, Taylor and Burgers, and the minimum rms error for the fit occurs at the same value of K/G. It can be seen that the Taylor displacement fields are a slightly better overall fit to the data over the entire range of K/G. Burgers' displacement fields represent the solution for a finite crystal free from surface tractions. The SEBM triblock analyzed exhibits a grained microstructure with grain sizes on the order of 5 μm—by no means an infinite crystal. However, it is likely that the grain boundaries do exert forces on each other; therefore, Taylor's solution evidently represents the more applicable one in this case. The minimum rms error for the system is seen at $K/G = 0.8 \pm 0.2$. Macroscopic tests on similar diblock copolymers have given a K/G ratio of 1.3−2.9.[39]

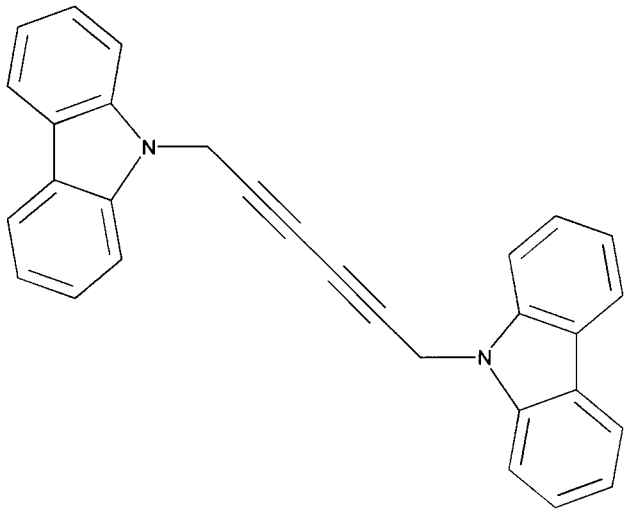

Figure 12. Carbazolyl-substituted diacetylene [1,6-di(*N*-carbazolyl)-2,4-hexadiyene] (DCHD).

Three Chain-End Edge Dislocation in DCHD

The carbazolyl-substituted diacetylene DCHD (Figure 12) can be polymerized in the solid state thermally or with electromagnetic radiation. Large crystals of the monomer (∼1 cm in length) can be precipitated from solution to form white, brittle crystals. When polymerized, the crystals undergo a quasi-homogeneous phase transformation to form gold, fibrous polymer crystals.[40,41] Direct images of the DCHD crystal lattice and individual dislocations in the lattice were first obtained by Read and Young.[42] An image of a three chain-end, $b[200] = 2.4$ nm, edge dislocation in a DCHD droplet is shown in Figure 13. The curvature of the droplet surfaces produces a low density of chain-end edge dislocations. This allows us to study isolated dislocations in detail. Seen in Figure 13 is the [010] projection of DCHD, and the 0.8 nm (200) planes are visible. The fringes correspond to the covalently bonded polymer chain, and the Burgers vector is perpendicular to the fringes. The directionality of these bonds along the chain, and the relatively weak lateral interactions between chains, give DCHD anisotropic mechanical properties.

To apply anisotropic dislocation theory to the problem, polyDCHD's 36 constant stiffness matrix, C_{ij}, was calculated using the molecular simulation software package Cerius^2 v 4.0. The Dreiding 2.21 force field[43] was used to minimize the energy of the system with convergence conditions of rms force $= 10^{-3}$ kcal/(mol Å). C_{ij} for DCHD polymer is shown in Table 1. Once referred to the reference frame of the dislocation, the stiffness matrix can be used to solve for the displacement fields u and v. These displacement fields are solved using linear elasticity and the compatibility equation method of solution. Substitution of the edge dislocation boundary conditions for an infinite elastic medium results in a sextic equation whose solution gives the complex roots p_n. Only in certain cases of high symmetry can an analytical solution be obtained. A chain-end dislocation in DCHD, which has a dislocation line x perpendicular to the dyad symmetry axis of the crystal, corresponds to one of these cases. The displacement fields for a dislocation in this orientation have been solved[44] and

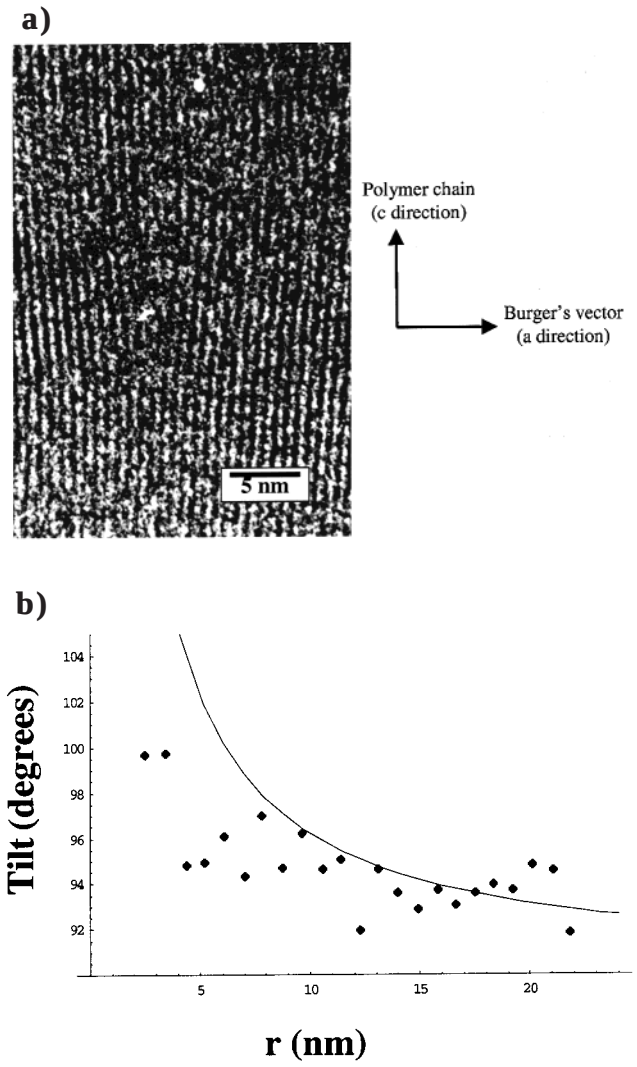

Figure 13. (a) HREM image of a $b[200] = 2.4$ nm three chain-end edge dislocation in the (010) projection of poly(DCHD). The fringes correspond to the (200) lattice planes. (b) Tilt of the (200) planes vs r at $\phi = 180°$. Anisotropic dislocation theory predicts a $1/r$ dependence. Theoretical tilt was calculated using the simulated stiffness matrix in Table 1.

Table 1. C_{ij} (GPa)

65.4	30.4	29.9	0	0	−1.86
30.4	74.3	34.1	0	0	0.01
29.9	34.1	113.9	0	0	13.0
0	0	0	30.5	18.7	0
0	0	0	18.7	23.3	0
−1.86	0.01	13.0	0	0	32.9

are shown below:

$$u[x,y] = \{(S_{11}{p_n}^2 + S_{12})B_n + S_{15}\gamma_n B_n\} \log[x + p_n y] \quad (10a)$$

$$v[x,y] = \{(S_{22}/p_n + S_{12}p_n)B_n + S_{25}\gamma_n B_n\} \log[x + p_n y] \quad (10b)$$

where p_n are the complex roots of the sextic equation, S_{ij} are the individual components of the rotated, reduced compliance matrix, γ_n is a relationship between the roots p_n and the compliance components, and B_n represents the influence of the magnitude and direction of the Burgers vector. Additional details of the solutions can be found elsewhere.[24,45]

With the displacements fields u and v calculated from this set of stiffness constants, we can study the tilt field of the dislocation in the image. The tilt of the (200) planes measured from the image is shown vs r in Figure 13b, along with the predicted tilt from anisotropic theory calculated using the stiffness components in Table 1. Tilt distortions calculated from anisotropic theory also scale as $1/r$ at constant ϕ moving away from the core. The deviation of the data from the theory at low r could be due to several factors. It is probable that inside a certain core radius r_0 linear elasticity cannot be assumed to be correct, and nonlinear effects are dominant. Traditional dislocation theory uses a cutoff radius, inside of which the stresses are greater than the theoretical shear strength of the material. Shear deformation in the slip plane of a chain-end dislocation in a polymer would involve rupture of covalent bonds, which is a very energetically costly process. DCHD has a high shear strength in planes perpendicular to the polymer chain, allowing us to measure tilt near the core. It is, however, likely that the tilt distortions we measure inside of r_0 do not conform to those predicted by linear elasticity.

Another possible explanation for the low degrees of tilt measured near the dislocation core could be contained in the details of the dislocation structure that are not readily visible in the raw image. Chain ends that do not terminate on the same (001) plane would give rise to lower chain tilt near the dislocation core. However, moving away from the core, the defect would be well approximated as a three chain-end, $b[200] = 2.4$ nm edge dislocation. Results from image filtering techniques have supported this hypothesis.

With these possibilities in mind, the dislocation core radius, r_0, was set at $r = 2b$. There is some precedent for the use of this distance as the core radius. Since the strains are of the order of $b/(2\pi r)$, Hooke's law will become invalid inside of $2b$.[46] By examining the dependence of the tilt measured from the image with increasing distance away from the core, we were able to make a direct estimate of the dislocation core radius, r_0, for a chain-end edge dislocation in DCHD. Measurements of the tilt taken from inside of $2b$ did not fit the predicted $1/r$ dependence of linear elasticity. For this reason, no measurements taken from inside of r_0 were used in the fit of the anisotropic displacement fields to the data. To fit the theory to the data, an anisotropy parameter, W_2, was defined:

$$W_2 = \frac{C_{11} + C_{33}}{2C_{55}} \quad (11)$$

The three most dominant stiffness constants for a dislocation in this particular crystallographic orientation are contained in the definition of W_2. C_{11} and C_{33} are the stiffness matrix components corresponding to principal stresses and strains, while C_{55} corresponds to shear stresses and strains. Variations in the magnitudes of all other stiffness constants had little effect on the predicted molecular displacements for this particular dislocation orientation. Figure 14 shows the plot of total rms error vs the anisotropy parameter W_2 for seven tilt data sets measured from the image. W_2 was changed by varying the magnitude of C_{55}, and a minimum rms error was found at $W_2 = 3.0 \pm 0.1$. This value illustrates the anisotropy of DCHD's mechanical properties. It

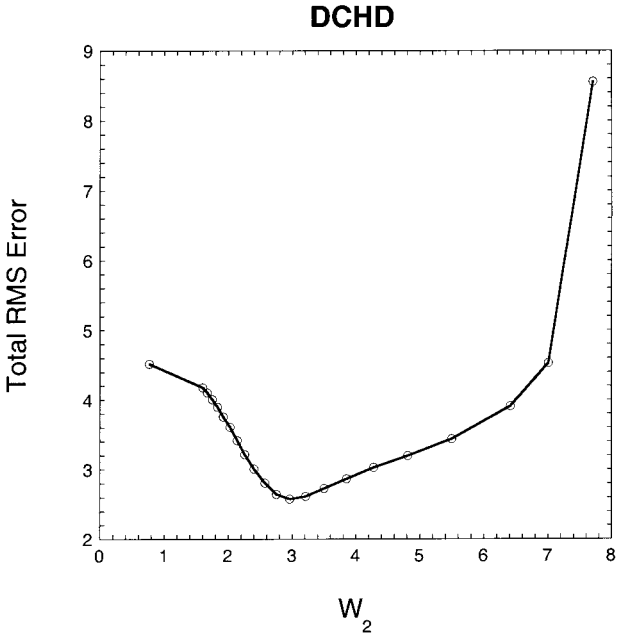

Figure 14. Graph shows total rms error plotted vs W_2, the anisotropy parameter. A minimum for the system was determined to be $W_2 = 3.0 \pm 0.1$.

implies that shear deformation is less energetically costly than principal deformation in this case. Considering the dislocation orientation, and the relative stiffness of the main chain, this is a physically reasonable conclusion. Figure 15 shows tilt vs ϕ plots at various values of W_2, illustrating the dramatic changes in the structure of the dislocation core with varying W_2. With decreasing shear modulus, C_{55} (increasing W_2), the amount of tilt deformation contained near the slip plane increases. As C_{55} approaches zero, tilt deformation becomes so localized near the slip plane that the model dislocation has effectively dissociated into two partial edge dislocations. As C_{55} increases, and shear deformation becomes difficult, the predicted tilt goes to zero. Here the strains are accommodated by simply forming a crack of width b. As seen in Figure 15a,c, these are poor fits to the measured data from the image. Figure 15b shows a representative data set of the best fit anisotropy parameter. In this figure $r = 4b$ and $W_2 = 3.0$.

Dislocations in Smectic Liquid Crystals

If the direction z is the director parallel to the layer normal in a smectic A liquid crystal, the free energy density for small displacements u in an absence of a magnetic field is[47−50]

$$F = \frac{1}{2}B\left(\frac{\partial u}{\partial z}\right)^2 + \frac{1}{2}k_{11}\left(\frac{\partial^2 u}{\partial x^2} + \frac{\partial^2 u}{\partial y^2}\right)^2 + \frac{1}{2}K'\left(\frac{\partial^2 u}{\partial z^2}\right)^2 + \frac{1}{2}K''\frac{\partial^2 u}{\partial z^2}\left(\frac{\partial^2 u}{\partial x^2} + \frac{\partial^2 u}{\partial y^2}\right) \quad (12)$$

The first term corresponds to the elastic energy for the compression (dilation) of the layers. The second term corresponds to the energy of splay deformation. It can be shown to be equal to the layer divergence (div **n**) where **n** is the layer normal. The last two terms are

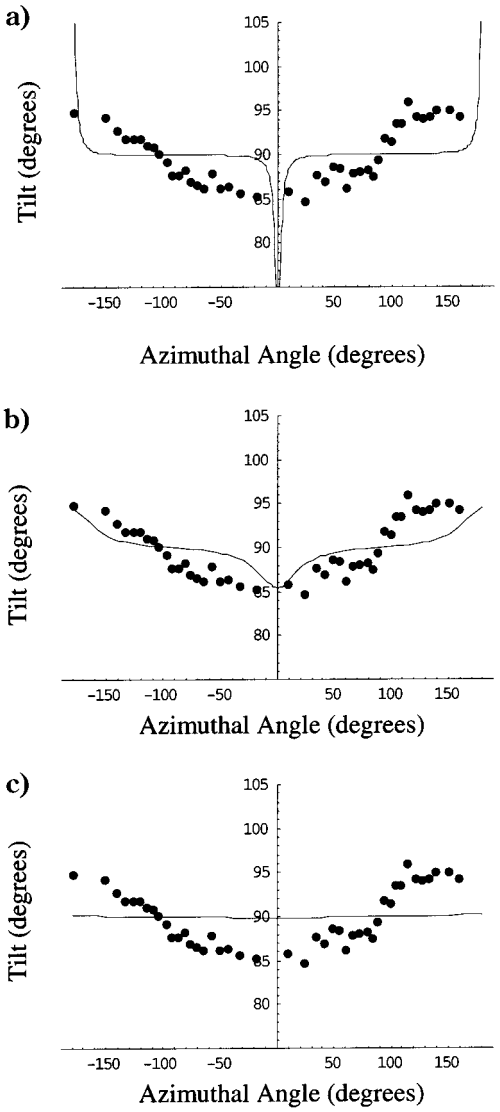

Figure 15. Theoretical tilt of the (200) planes vs azimuthal angle is shown with the measured data at $r = 4b$ for various values of W. (a) $W_2 = 7.7$, (b) $W_2 = 3.0$, (c) $W = 0.8$.

negligible and can be ignored, giving

$$F = \frac{1}{2}B\left(\frac{\partial u}{\partial z}\right)^2 + \frac{1}{2}k_{11}\left(\frac{\partial^2 u}{\partial x^2} + \frac{\partial^2 u}{\partial y^2}\right)^2 \quad (13)$$

For an edge dislocation with a dislocation line along y, there are no displacements in the y direction. Taking u to be independent of y gives

$$F = \frac{1}{2}B\left(\frac{\partial u}{\partial z}\right)^2 + \frac{1}{2}k_{11}\left(\frac{\partial^2 u}{\partial x^2}\right)^2 \quad (14)$$

The equation of equilibrium can be found by minimizing the energy with respect to u.

$$B\frac{\partial^2 u}{\partial z^2} - \lambda^2\frac{\partial^4 u}{\partial x^4} = 0 \quad (15)$$

where

$$\lambda = [k_{11}/B]^{1/2} \quad \text{and} \quad u = u[z,x]$$

Substituting the boundary conditions for an edge dis-

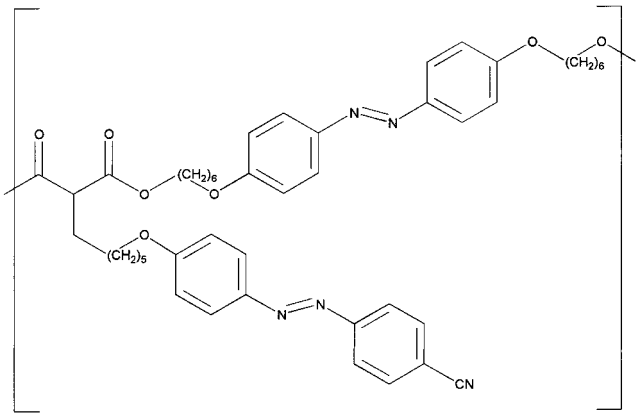

Figure 16. Main chain/side group liquid crystalline polymer polymalonate.

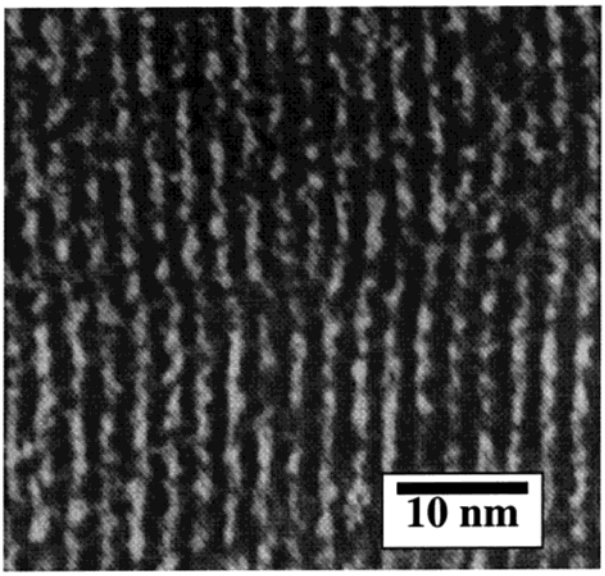

Figure 17. A $b = 2.6$ nm edge dislocation in smectic polymalonate.

location, the tilt (θ) and dilation (δ) of the layers can be derived.

$$\theta = \frac{\partial u}{\partial x} = \frac{1}{4\pi^2}\frac{b}{(\lambda z)^{1/2}}\exp\left(\frac{-x^2}{4\lambda z}\right) \qquad (16)$$

$$\delta = \frac{\partial u}{\partial z} = \frac{1}{8\pi^{1/2}}\frac{b}{(\lambda z)^{3/2}}\exp\left(\frac{-x^2}{4\lambda z}\right) \qquad (17)$$

The deformation of smectic A materials can be described in terms of a characteristic deformation length, λ, which depends on the splay modulus k_{11} (units energy length^{-1}) and the elastic modulus B (units energy length^{-3}). The parameters needed to define the tilt, θ, of the layers are b, the Burgers vector of the dislocation, and λ, the characteristic length.

We have studied edge dislocations in the main chain/side group liquid crystalline polymalonate (Figure 16). Figure 17 shows a $b = 2.6$ nm edge dislocation in a smectic polymalonate.[51] To determine λ from this particular HREM image we have mapped out the tilt field ($\theta[x,y]$) of the smectic layers near the defect. Using the above equation for tilt, θ, and by defining b and varying λ, it is possible to find the best fit of the data to the theory. A minimum for this system was determined to be $\lambda = 1.1 \pm 0.1$ nm, giving $(K_{11}/B) = 1.2$ nm^2.

Conclusions

We have investigated the elastic properties of edge dislocations in various polymeric materials by comparing experimental results using TEM and HREM to the expected distortions predicted by dislocation theory. A novel method was developed for this analysis to measure the tilt, θ, of the polymer lattice planes and compare the results to tilt calculated from the theoretical displacement fields. A $b[020] = 63$ nm edge dislocation in the knitted structure of PS-*block*-PEB-*block*-PMMA was found to conform to the elastic properties of an isotropic dislocation. The displacement fields according to Taylor proved to be a slightly better fit to the data than those according to Burgers. The ratio of the bulk modulus to the shear modulus, K/G, was found to be near 0.8 ± 0.2. Further investigations of the deformation fields near isotropic dislocations gave insight into the changes of the core structure with changes in K/G. Anisotropic dislocation theory was used to model a three chain-end edge dislocation in DCHD. An anisotropy parameter, W_2, was defined and found to be equal to 3.0 ± 0.1. This value illustrates that the shear deformation is preferred over principal deformation for a chain-end edge dislocation in DCHD. Finally, a dislocation in a smectic liquid crystal was modeled using liquid crystalline theory. The characteristic length, λ, was determined to be equal to 1.1 ± 0.1 nm.

Acknowledgment. The authors thank the Alexander von Humboldt Foundation, the Max Planck Institute for Polymer Research, the National Science Foundation DMR-0084304, DMR-9707975, and the NSF sponsored IGERT program for Molecularly Designed Electronic, Photonic and Nanostructured Materials at the University of Michigan.

References and Notes

(1) Martin, D. C.; Thomas, E. L. *Mater. Res. Soc. Bull.* XII **1987**, *8*, 27.
(2) Martin, D. C.; Thomas, E. L. *Polymer* **1995**, *36*, 1743.
(3) Voigt-Martin, I. G. *Acta Polym.* **1996**, *47*, 311.
(4) Tsuji, M.; Kohijiya, S. *Prog. Polym. Sci.* **1995**, *20*, 259.
(5) Hudson, S. D. *Curr. Opin. Colloid Interface Sci.* **1998**, *3*, 125.
(6) Kübel, C.; Martin, D. C. *Philos. Mag. A* **2001**, *81*, 1651.
(7) Vitek, V. *Prog. Mater. Sci.* **1992**, *36*, 1.
(8) Amelinckx, S.; Delavignette, P. *Direct Observation of Imperfections in Crystals*; Interscience: New York, 1962.
(9) Audrier, V.; Demenet, J. L.; Rabier, J. *Philos. Mag. A* **1998**, *77*, 843.
(10) Keith, H. D.; Passaglia, E. *J. Res. Natl. Bur. Stand.* **1964**, *68*(A), 513.
(11) Predecki, P.; Statton, W. O. *J. Appl. Phys.* **1966**, *37*, 4053.
(12) Shadrake, L. G.; Guiu, F. *Philos. Mag.* **1976**, *34*, 565.
(13) Peterson, J. M. *J. Appl. Phys.* **1966**, *37*, 4047.
(14) Young, R. J. *Philos. Mag.* **1974**, *30*, 85.
(15) Young, R. J. *Mater. Forum* **1988**, *11*, 210.
(16) Brooks, N. L.; Mukhtar, M. *Polymer* **2000**, *41*, 1475.
(17) Hudson, S. D.; Fleming, J. W.; Gholz, E.; Thomas, E. L. *Macromolecules* **1993**, *26*, 1270.
(18) Hudson, S. D.; Thomas, E. L. *Phys. Rev. Lett.* **1989**, *62*, 1993.
(19) Hobdell, J.; Windle, A. *Liq. Cryst.* **1997**, *23*, 157.
(20) Ries, R.; Lieser, G.; Schwiegk, S.; Wegner, G. *Acta Polym.* **1997**, *48*, 536.
(21) Ide, N.; Okada, I.; Kojima, K. *J. Phys.: Condens. Matter* **1993**, *5*, 3151.
(22) Mokichev, N. N.; Pakhomov, L. G. *Sov. Phys. Solid State* **1982**, *24*, 1925.
(23) Kübel, C.; González-Ronda, L.; Drummy, L. F.; Martin, D. C. *J. Phys. Org. Chem.* **2000**, *13*, 816.
(24) Wilson, P. M.; Martin, D. C. *Macromolecules* **1996**, *29*, 842.

(25) Auschura, C.; Stadler, R. *Polym. Bull.* **1993**, *26*, 2171.
(26) Wilson, P. M.; Martin, D. C. *J. Mater. Res* **1992**, *7*, 3150.
(27) Yee, K. C.; Chance, R. R. *J. Polym. Sci.* **1978**, *16*, 431.
(28) Voigt-Martin, I. G.; Durst, H. *Macromolecules* **1989**, *22*, 168.
(29) Taylor, G. I. *Proc. R. Soc. London* **1934**, *145*, 362.
(30) Read, W. T. *Dislocations in Crystals*; McGraw-Hill: New York, 1952.
(31) Hirth, J. P.; Lothe, J. *Theory of Dislocations*, 2nd ed.; Wiley-Interscience: New York, 1982.
(32) Chaikin, P. M.; Lubensky, T. C. *Principles of Condensed Matter Physics*; Cambridge University Press: Cambridge, 1995.
(33) Burgers, J. M. *Proc. K. Akad. Amst.* **1939**, *42*, 263.
(34) Koehler, J. S. *Phys. Rev.* **1960**, *60*, 397.
(35) Nabarro, F. R. N. *Adv. Phys.* **1952**, *1*, 269.
(36) Weertman, J.; Weertman, J. R. *Elementary Dislocation Theory*; Macmillan: New York, 1964.
(37) Hull, D.; Bacon, D. J. *Introduction to Dislocations*; Butterworth-Heinemann: Oxford, 1984.
(38) Breiner, U.; Krappe, U.; Thomas, E. L.; Stadler, R. *Macromolecules* **1998**, *31*, 135.
(39) Arridge, R. G. C.; Folkes, M. J. *J. Phys. D* **1972**, *5*, 344.
(40) Enkelmann, V.; Leyrer, R. J.; Schleier, G.; Wegner, G. *J. Mater. Sci.* **1980**, *15*, 168.
(41) Liao, J.; Martin, D. C. *Philos. Mag. A* **1996**, *74*, 195.
(42) Read, R. T.; Young, R. J. *J. Mater. Sci.* **1984**, *19*, 327.
(43) Mayo, S. L.; Olafson, B. D.; Goddard, W. A. *J. Phys. Chem.* **1990**, *94*, 8897.
(44) Steeds, J. W. *Anisotropic Elasticity Theory of Dislocations*; Clarendon Press: Oxford, 1973.
(45) Nye, J. F. *Physical Properties of Crystals*; Clarendon Press: Oxford, 1957.
(46) Nabarro, F. R. N. *Theory of Crystal Dislocations*; Dover Publications: New York, 1987.
(47) Chandrasekhar, S. *Liquid Crystals*; Cambridge University Press: Cambridge, 1992.
(48) De Gennes, P. G.; Prost, J. *The Physics of Liquid Crystals*; Clarendon Press: Oxford, 1993.
(49) Landau, L. D.; Lifshitz, E. M. *Theory of Elasticity*; Pergamon Press: New York, 1986.
(50) Kleman, M.; Oswald, P. *J. Phys. (Paris)* **1982**, *43*, 655.
(51) Voigt-Martin, I. G.; Durst, H. *Macromolecules* **1989**, *22*, 168.

MA010003B